Basalt-polypropylene fiber reinforced concrete for durable and sustainable pipe production. Part 1: Experimental Program

Zhiyun Deng[a,b], Xinrong Liu[a,b*], Peng Chen[a,b], Albert de la Fuente[c*], Xiaohan Zhou[a,b*], Ninghui Liang[a,b], Yafeng Han[a,b], Libing Du[a,b]

[a] School of Civil Engineering, Chongqing University, Chongqing 400045, China

[b] National Joint Engineering Research Center of Geohazards Prevention in the Reservoir Areas(Chongqing), Chongqing 400045, China

[c] Civil and Environmental Engineering of UPC BarcelonaTECH, Jordi Girona 1-3, 08034 Barcelona, Spain

* Corresponding authors.

E-mail address: Xinrong Liu, liuxrong@126.com; Albert de la Fuentec, albert.de.la.fuente@upc.edu; Xiaohan Zhou, zhouxh2008@126.com

Abstract: An experimental program consisting in producing and testing reinforced concrete pipes (RCPs) under the three-edge bearing tests considering different types of reinforcement was carried out. Four types of RCPs were produced, these reinforced with: (1) polypropylene macrofibers; (2) basalt microfibers; (3) combination of both (hybrid reinforcement) and (4) plain concrete. The analysis of the crack patterns and both service and ultimate mechanical responses allowed concluding that the use of fibers do not lead to an effective increase of the first cracking load; however, both types of fibers allowed a better crack width control respect to the standard reinforced concrete pipe. In this regard, basalt microfiber reinforced concrete led to a better response caused by concentrated loads (jacketing) whilst polypropylene macrofibers increased the concrete pipe performance in terms of bearing capacity and flexural crack control. The hybrid fiber reinforced concrete was found to be the most suitable alternative for increasing the load bearing capacity and the crack width control for service loads. These incipient experimental results permit to conclude that this type of hybrid basalt-polypropylene fiber reinforced concretes are an interesting alternative to traditional steel-cage reinforced concrete pipes.

Keywords: Basalt-polypropylene fiber reinforced concrete; Fiber reinforced concrete pipe; Three-edge bearing test; Mechanical response; Post-cracking strength

1 Nomenclature

b: The pipe length

B: Basalt

B-PP: Basalt-polypropylene

B–PPF: Basalt-polypropylene fiber

BF: Basalt fiber

C_f: Amount of fibers (kg/m^3)

D： Double reinforcement cages

D_i: Internal pipe diameter

DL: Normalized pipe load-carrying capacity ($P/(L \cdot D_i)$)

D_{cr}: Crack load of DL when crack first appear

$D_{0.3}$: Service load of DL when crack width is 0.3 mm

D_u: Ultimate load of DL

E_{post}: Energy released in a region comprised between δ_{peak} and δ

f_{cc}: Concrete compressive strength (MPa)

$f_{ct,R}$: Post-cracking residual strength to concrete

f_{ct}: Concrete tensile strength (MPa)

$f_{ct,fl}$: Flexural tensile concrete strength

PCP: Plain concrete pipe

P_{cr}: Cracking load of the pipe

P_u: Ultimate load of the pipe

FRCP: Fiber reinforced concrete pipe

h: The pipe wall thickness

HFRCP: Hybrid fiber reinforced concrete pipe

IT： Impact test

MAP： Numerical model for the analysis of pipes

L: Pipe length

L_{cl}: A half of the pipe circumferential length ($\pi D_i/2$)

LLT： Live loads test

LTLT：Long-term loading tests

MAP: Model for the Analysis of Pipes

No.: Number

P: Pipe load

$P_{0.3}$: Load-carrying capacity of 0.3 mm crack width

P_u: The maximum load-carrying capacity

RCP: Reinforced concrete pipe

PP: Polypropylene

PPF: Polypropylene fiber

PCS: Post-cracking strength

P_{peak}: Peak PCS

PFRCP: Polypropylene fiber reinforced concrete pipe

PVA: Polyvinyl alcohol

Ref.: Reference

S: Steel

Si：Single reinforcement cage

SF: Steel fiber

SFRCP: Steel fiber reinforced concrete pipe

SPP-HRCP: Steel-polypropylene hybrid fiber reinforced concrete pipe

TEBT：Three edge bearing tests

w_{max}: The maximum crack width of pipe subjected to $D_{0.3}$

Φ_f: Diameter of the fiber (mm)

λ_f: The fiber aspect ratio

δ: Deflection

δ_{peak}: Deflection of P_{peak}

1. Introduction

Pipe jacking is a trenchless pipeline construction technology (see Fig.1) which is widely used in several fields, such as oil and gas transmission, municipal sewage pipelines and hydraulic engineering, among others. The pipes, besides the service loads (flexural forces that govern the mechanical requirements), should withstand a transient thrust force during jacketing that can lead to high compressive forces and, thus, to splitting and spalling concrete cracks.

Concrete is the predominant material for producing these type of pipes, Reinforced Concrete Pipe (RCP) technology being widely used in storm sewer systems and other applications for pipelines. [1] Nevertheless, aspects related to construction (ex., unexpected thrust magnitudes and/or higher eccentricities than those considered in the design, together with challenging geological conditions) and other challenges associated with reinforced concrete limitations (ex., limited tensile strength of the material), make the pipes prone to cracking during construction; furthermore, the width of these cracks can increase during service life due to the operational loads and, as consequence, pathologies derived from concrete and/or steel are likely to occur (see Fig. 2).

The cracks presented in Fig. 2 are frequent and its occurrence is governed by the concrete tensile strength (f_{ct}) and the transient/service loads and not by the amount of steel rebar reinforcement. Alternatively, the use of structural fibers as concrete reinforcement has proved to be an effective way to enhance the crack control of pipes and, as a consequence, to improve durability and serviceability of these elements. [2]

Steel macrofibers have been predominantly accepted in concrete pipes for replacing the steel rebar cages historically and widely used for reinforced concrete for pipes (RCPs) [3-6]. In this regard, steel fiber reinforced concrete (SFRC) has been confirmed to be a suitable material for crack width control in concrete pipes and capable to provide the required load bearing capacity in a wide range of pipe strength classes. [7-14]

Nonetheless, due to the material composition of steel fibers (SFs), these are prone to suffer from corrosion and, thus, to jeopardize the durability of the pipes. This aspect can be especially problematic in chloride environments (ex., soils with water table contaminated by saline intrusion). Likewise, the addition of SFs reduces the concrete workability and admixtures (plasticizers and superplasticizers) must be added to compensate the loss of workability, this increases the material cost. Alternatively, structural synthetic macrofibers have emerged as an alternative non-metallic reinforcement capable of providing post-cracking residual strength to concrete ($f_{ct,R}$). The main advantages of using synthetic macrofibers as concrete reinforcement are: (1) minor impact on the workability of the fresh concrete; (2) these are inert to chlorides and aggressive chemicals that can affect to steel reinforcement and/or concrete [15-17] and (3) in case of fibers remain at surface of the pipes, these hardly can cause injuries to labors due to its flexibility. Some authors [18-22] have even concluded that polypropylene macrofibers (PPFs) can be more efficient (for a certain range of fiber volumes and mechanical requirements) than SFs for increasing toughness and post-cracking residual strength of concrete.

For these reasons, FRC has been already examined as a potential structural material to produce pipes. In this regard, Table 1 gathers the main features of those experimental and numerical research related to fiber reinforced concrete pipes (FRCPs).

Table 1 allows confirming that there exists extensive research (experimental and numerical) on FRCPs and that this topic is of interest from both scientific and industrial perspective. Additionally, it must be remarked that Peyvandi et al. [34, 35] have put forward a design-oriented approach for concrete pipes with PVA (polyvinyl alcohol) fibers and steel fibers. Mohamed et al. [11, 12, 28] have investigated on the mechanical performance SFRCPs by means of full-scale tests. Park et al. [36-38] have also researched on the structural performance of concrete pipes with PPFs, PPFs and reduced traditional steel cage, and steel and synthetic fibers. The general conclusion that can be extracted from the previous research is that the use of structural fibers, steel and/polypropylene, as unique concrete reinforcement or in combination with a minimum amount of steel rebars is technically feasible and a competitive solution in front of RCPs.

The hybridization of different types of fibers has also been investigated, steel and synthetic (polypropylene) fibers having been analyzed as concrete reinforcement and its properties experimentally characterized. [18, 33, 39, 40] In this sense, hybrid steel-synthetic fiber reinforced concrete pipes (HFRCPs) have proven to perform at similar, or even at higher level, in comparison to RCPs. [38] Particularly, Park et al. [38] analyzed the enhancement of the structural performance of concrete pipes with internal diameters (D_i) ranging from 600 to 900 mm through the use of crumb rubber, steel (S), and polypropylene (PP) fibers. This research concluded that hybrid S and PP fibers were more effective than single PP or S fibers in enhancing the strength and ductility of rubberized concrete pipes. Lee et al. [41] discussed the mechanical responses of SPP-HRCPs. The pipe diameters in this study ranged from 375 to 900mm for synthetic FRCPs and 450 to 900mm for SFRCP. All pipes had Class III compressive strength and type B wall thickness in accordance with the ASTM C76 Standard specification. [3] This study concluded that a fiber volume ranging between 0.15 and 0.20% allow reaching the maximum strength capacity. Despite the advantages of these HFRCs, this material is still sensitive to corrosion of SFs and, hence, the durability and serviceability can be compromised to some extent.

Alternatively, basalt microfibers (BFs) have been found to be an appropriate structural inorganic fiber to partially replace the metallic reinforcement attractive mechanical and physical properties, such as: high temperature stability; tensile strengths ranging from 992.4 MPa [42] to 4800MPa [43] together with appropriate ductility; good acid and alkali-resistance [42-46]. Fu et al. [47] already pointed out that BFs can be used, in combination with PP microfibers, as a partial (or even total in case of low design loads) substitute of metallic reinforcement with benefits related to the cracking control and the fire resistance. Nonetheless, the research on the used hybrid basalt and polypropylene fibers with structural purposes is limited and much focused on behavior against impact [47-49] and toughness [50] and flexural properties [51] of B–PPFs; however, the PPFs used in those researches were non-structural microfibers and, thus, the potential post-cracking strength enhancement owe to the combination of B-PP microfibers is missed. It must be also emphasized that basalt is an eco-friendly material. [52]

To the authors' best knowledge, there is no previous research on the mechanical properties of concrete pipes reinforced with hybrid of BS and PP (micro- and macrofibers, respectively). In this sense, the combined use of both fiber types is expected to lead to synergetic effects as reinforcement for concrete pipes since BFs can enhance the crack performance in service while PPFs can increase both load bearing capacity and ductility of the pipe. Both features are of great interest for pipes with D_i larger than 1000 mm, and for which the steel-cage reinforcement cannot be fully replaced by structural fibers due to the high operational loads to be resisted. For those, the addition of fibers resistant to aggressive environments and capable to provide an effective crack width control when pipes are subjected to the service loads could reduce the problems related to steel rebars corrosion (pathology governed, among other, by the crack width).

To this end, an experimental program involving the production and testing of 1.0 m internal diameter steel reinforced concrete pipes considering the combination of BFs, PPFs and B-PPFs was carried out. The results are presented and analyzed herein, giving special attention to the crack patterns and the maximum load capacity of each tested pipe. The results and conclusions are expected to increase the confidence of designers towards this composite material.

2. Experimental program

2.1. Materials

Embossed PP macrofibers (Fig. 3(a)) together with B microfibers (Fig. 3(a)) were used. The length and diameter of the former was 50 mm and 0.8 mm, respectively, with a modulus of elasticity of 7.4 GPa and tensile strength of 706 MPa. The basalt microfiber presented a length of 19 mm and a diameter of 0.013 mm, the tensile strength of this fiber ranging from 3300 to 4500 MPa and the modulus of elasticity from 95 to 115 GPa. See Table 2 for further details of the fibers.

Portland cement P.O 52.5 was used as binder, the skeleton of the concrete matrix consisting of coarse aggregates with sizes ranging from 10 to 20 mm and 5 to 10 mm together with 0~5 mm particle size river sand. A commercial polycarboxylic acid superplasticizer was included to guarantee the required workability. This concrete dosage was designed to guarantee a compressive concrete strength (f_{cc}) of 50 N/mm^2. The concrete dosage is shown in Table 3.

2.2. Reinforcement

The steel reinforcement layout depicted in Fig. 4 was used in all pipes. This consisted in a double-cage of 400 N/mm^2-yielding tensile strength steel reinforcement 8 mm-diameter circular bars each 100 mm, the concrete cover being 27 mm and 20 mm for the outer and inner layer, respectively.

A total of four concrete pipes were produced: (1) standard RCP; and RCPs with (2) BFs; (3) PPFs, and (4), with hybrid B-PPFs. Details about the coding and the amount and type of fibers used in each pipe, along with the compressive (f_{cc}) and tensile (f_{ct}) concrete strengths [53] are gathered in Table 4.

As shown in Table 4, fiber contents ranged between 0 and 6 kg/m^3. Amount of 4 kg/m^3 of PP fibers was considered the lower bound to provide ductility of the composite respect the unreinforced concrete [54, 55] whilst 6 kg/m^3 was fixed as an upper bound since higher amounts, although possible, could have compromised the workability and the finishing [7, 8, 26].

2.3. Mold and pipe production

In order to produce the pipe that can meet the requirements of the laboratory test, a mold for pipe production (Fig. 5) was specifically designed for this research.

As shown in Fig. 5, the system consisted of a horizontal base (1) which supported both external (8) and internal (10) molds. The circular molds were fabricated independently by the union of two semicircle pieces each of those formed by vertical 1 m-length wooden blocks uniformly spaced each 3 cm; these wrapped by means annular iron straps, (7, ext.) and (13, int.), of 3 mm of thickness. Reinforcing formworks were added, see (6) and (14). The whole formwork system was connected through a nail (12). The external annular reinforcement device consisted of the reinforcing formworks (6) and the iron hoops

(5), both uniformly distributed along the direction of height. For the internal annular reinforcement device only a reinforcing formwork (14) was installed. Both annular reinforcement devices ensured uniform pipe thickness. Aiming at guaranteeing stability and stiffness of the system, the two external semicircle molds (6) were connected through the wooden blocks (4) and the nails (12). The connecting wood blocks (4) were removed to allow the removal of the external mold. As for the internal mold, in addition to connecting the internal reinforced formworks (14) through the wood blocks at the joint, rubber strip (11) was also set at the joint of the two internal semicircle molds. Thus, the space for removing the internal mold could be realized when the rubber strip was pulled out.

All four pipes were manufactured with the self-designed mold shown in Fig. 5. Part of pipe production processes are shown in Fig. 6. The production process of pipes (Fig. 6) was as follows:

① Install and position the internal mold, and fix the internal annular reinforcement device

② Position the steel cage

③ Install and position the external mold, and fix the external annular reinforcing device

④ Mix the concrete mixture

Firstly, the pre-weighed coarse and fine aggregates were poured into the forced mixer, which was wet but no clear water on the surface, and mixed for 1 minute; secondly, evenly scatter the polypropylene and/or the BFs were included into the mixer, and the mixing continued for about 2 minutes; thirdly, the cement was poured and mixed during a 1 minute with the previous components; and, finally, the water and water reducer agent was slowly and evenly poured into the mixer and the material was mixed for 2 minutes.

⑤ Layered pouring and vibrating

The mixture was poured into the annular gap (9) of the self-designed mold. In this process, layered pouring and layered vibrating method was carried out to ensure that the concrete was properly compacted.

⑥ Specimen curing

Four specimens were poured on the same day and demold after 24 hours. The covering-watering method was resorted to cure the specimens. The mechanical tests were conducted after 28 days of curing.

After the production of the pipes, the wall thickness of the pipe was measured, this being of 100 ± 1.0 mm. In addition, no honeycomb or pitting surface was observed during the visual inspections. Thus, both pipe's geometry and finishing were found to be adequate to be accepted within a quality control process. Hence, the self-designed mold proposed in this paper proved to be suitable for producing these pipes. Also, a related Chinese patent titled "the casting mold for a large diameter concrete pipe" (201921940203.3) was applied.

2.4. Three-edge bearing test

The mechanical capacity of the produced pipes was characterized by means of performing worldwide accepted three-edge bearing test (Fig. 7). According to the ASTM C76 [3] specifications, the tests consist in supporting the pipe onto longitudinal strips (Fig. 7(a)), and applying onto the crown a load uniformly distributed along the pipe length using an upper bearing strip (Fig. 7(b)).

This test configuration is designed to characterize the bearing capacity under the most unfavorable both load (punctual) and support boundary conditions (no lateral passive/active soil pressure and minimum width of the supporting rigid bed). The results derived from the tests are considered as reference to define the pipe strength class (Table 5).

In this sense, both the 0.3 mm crack width ($P_{0.3}$) and the maximum (P_u) load-carrying capacities are measured during the test. These loads are normalized as $DL = P/(L \cdot D_i)$ (kN/m^2), L and D_i being the length and the internal diameter of the pipe, respectively, and finally compared to those gathered in Table 5 for the target pipe strength class.

For this research, and aiming at assessing up to which extend the contribution and effects on the resistant mechanism due to the addition of fibers in a high structural pipe is effective, the V strength class ($D_{0.3}$ = 140 kN/m^2 and D_u = 175 kN/m^2) was targeted. In this regard, it must be remarked that the steel-cage configuration presented in Fig. 4 was designed to guarantee the pipe strength class V; therefore, the use of fibers was meant to increase the load-bearing capacity and, particularly, to reduce the crack width (accepted up to 0.3 mm) for service loads and, with that, increase the pipe durability.

The tests (Fig. 8) were carried out by applying a uniform loading rate of 1.8 kN/s up to reaching 75% of the service load ($D_{0.3}$ = 140 kN/m^2) and of 0.7 kN/s until detecting the maximum load. Beyond this point, the load level was controlled by displacement to measure continuously post-failure response of the pipe. A computer-based data acquisition system was used to record the applied load. The crack patterns (number and width) at crown, invert and springline of the pipe (Fig. 8(b)) were monitored. Cracks were monitored with a crack tester (Fig. 8(c)), and displacements were measured by means of a

DongHua DH3816N device (Fig. 8(d)).

3. Experimental results and discussion

3.1. Cracking loads and crack patterns for service loads

The normalized load DL versus the vertical deflection measured at the crown for each pipe are presented in Fig. 9.

Based on Fig. 9, it is remarkable that the shape of load-deflection curve of the standard RCP (B0P0) is similar to that of fiber reinforced specimens (B0P6, B6P0 and B2P4). This can be attributed to the fact that steel cage determines both the global response and the bearing capacity of the pipe, whilst fibers permits to enhance the bearing capacity from cracking to post-failure (included) as it is discusses above.

The cracking of the pipes occurred at the inner face of the crown for a load (D_{cr}) that ranges from 70 to 80 kN/m^2. This allows confirming that the effect of fibers in the resistant mechanism is only active once the concrete cracks, the flexural tensile concrete strength ($f_{ct,fl}$) being governed exclusively by the concrete matrix strength. Therefore, fibers (with this size and amount) are confirmed not to alter the pre-cracking response of the pipe.

Right after the first crack appeared at the crown, another occurred at the invert section (also at the inner face). As the load increased to approximately 80 to 90 kN/m^2, two longitudinal cracks occurred at the springline (outer faces) of the pipe specimens. These sections are subjected to a combination of bending moment (including the redistributed bending moment caused by the cracking at crown and invert sections) and axial compressive force. The four initial cracks remain the largest cracks in terms of crack width throughout the loading process. Subsequent loading generated secondary cracks, which were distributed at both sides of the four main cracks.

Fig. 10 shows the external crack patterns of the four pipe specimens after unloading.

In Fig. 10 each crack is numbered and the load level at which the crack occurs is marked. At the same time, the crack width of each crack is monitored during the whole loading process. Besides, the maximum width of the four main cracks and the average crack width of the secondary cracks at each load level for each key section were also calculated. Table 6 gathers the information of cracks for each key section of the four pipes when subjected to the service load ($D_{0.3}$ = 140 kN/m^2).

Based on the results presented in Fig. 10 and Table 6, it can be noticed that the density of cracks increase with the addition of fibers. In this regard, the addition of 6 kg/m^3 of PPFs (B0P6) and the hybridization of 2 kg/m^3 (BFs) and 4 kg/m^3 (PPFs) considered for the pipe (B2P4) allowed increase the number of cracks at the springline (12 and 9 at the right, while 11 and 8 at the left) with respect to the traditional RCP (B0P0), which presented 4 and 5 cracks at right and left springline, respectively. It must be noticed that the wider cracks appeared at the inner face of the crown, the greater maximum crack width (w_{max}) being 0.39 mm for the B0P0 subjected to $D_{0.3}$ (140 kN/m^2). Thus, this pipe would not fulfill the service requirement for $D_{0.3}$ (140 kN/m^2) as the maximum allowed crack width is limited to 0.30 mm for this load level. Nevertheless, the positive effect of fibers, which proved to be effective for controlling the opening of the crack width, led to w_{max} of 0.18 mm (B0P6), 0.26 mm (B6P0) and 0.17 mm (B2P4). And consequently, the FRCPs are compliant with the standards for $D_{0.3}$ in terms of crack width.

Fig.11 depicts the relationship w_{max} – DL for the tested pipes. In this regard, it is evident that the contribution of the fibers in controlling the crack extended up to failure. In fact, the inclusion of 6 kg/m^3 of BFs (B6P0) led this pipe to reach the strength class V with a $D_{0.3}$ = 148 kN/m^2 (5.7% and 17.4% superior to the $D_{0.3}$ specified for a strength class V and to the $D_{0.3}$ reached by the pipe P0B0, respectively) and, hence, this basalt microfiber size and amount (Table 2) proved to be effective for controlling cracks with widths of this magnitude. The addition of 6 kg/m^3 of PPFs (B0P6) and the hybridization of 2 kg/m^3 (BFs) and 4 kg/m^3 (PPFs) considered for the pipe (B2P4) allowed reaching $D_{0.3}$ of 165 kN/m^2 (17.8% and 30.9%) and 169 kN/m^2 (20.7% and 34.1%). This increment of 3.0% for the $D_{0.3}$ detected for the specimen B2P4 respect to B0P6 might be due to a positive synergetic effect caused by the hybridization of fibers; nonetheless, this statement must be considered as a prelaminar conclusion due to the limited number of tests and variability could be hiding other phenomena.

3.2. Failure and post-failure response

According to the results gathered in Fig. 9, the ultimate (peak) loads (D_u) were detected for a vertical displacement (δ_{peak}) comprised within a range between 18 to 20 mm; thus, δ_{peak} is independent on the fiber reinforcement considered but rather on the steel cage configuration. Contrarily, D_u resulted to be sensitive to both type and amount of fibers.

In this regard, the D_u for the B0P0 (reference RCP) was 216 kN/m^2, the D_u specified for a pipe strength class V being 175 kN/m^2; therefore, this represented a 23.4% overdesigned failure load capacity. This was expected to occur since the steel bar reinforcement amount is determined by the 0.3 mm crack width load condition ($D_{0.3}$ = 140 kN/m^2) required for the strength class V. Nevertheless, as discussed in section 3.1, this reinforcement configuration (Fig. 4) is insufficient for fulfilling this limitation. The inclusion of the fibers to this RCP allowed to reach the pipe strength class V without adding more steel bars, which make these FRCPs less prone to suffer from corrosion in aggressive environments.

As for the D_u registered for the FRCPs, these were 243, 271 and 282 kN/m^2 for the specimens B6P0, B0P6 and B2P4, respectively, and greater than the D_u of 175 kN/m^2 required for a strength class V. Consequently, there was an increase of D_u ranging from 12.5% (B6P0) to 31.0% (B2P4) respect to that obtained for the RCP of reference (216 kN/m^2). By means of comparing the D_u values achieved by the pipes B0P0 and B6P0 (see Fig. 9), that BFs showed mechanical performance even at this load regime, for which the crack widths were up to 3 mm and there were already evidences of fiber pull-out. On the other hand, the polypropylene macrofibers showed a suitable bond performance owe to the embossed surface and good mechanical compatibility with the concrete matrix. Finally, it is noticeable that there was a structural positive synergetic effect due to hybridization of the fibers since, for the same total amount of fibers (6 kg/m^3 each pipe), there was an increase of D_u for the pipe B2P4 of 16.0% and 4.1% respect to the pipes B6P0 and B0P6, respectively.

In order to complement this structural analysis, despite the pipelines standard only specify requirements in terms of load bearing capacity, the post-failure energy abortion capacity is assessed by following the procedure proposed by Banthia and Trottierin [56]. These authors suggested the use of the Eq. (1) to compute the parameter of post-cracking strength (PCS), which involves the quantification of the energy associated with the post-failure mechanism and other deformational and geometric variables. This approach was also considered by Mohamed et al. [11] for quantifying the ductility capacity of the pipes for design purposes.

$$PCS = \frac{(E_{post})L_{cl}}{(\delta - \delta_{peak})bh^2} \tag{1}$$

where, L_{cl} is half of the pipe circumferential length ($\pi D_i/2$); δ is deflection and δ_{peak} is the deflection of P_{peak} and E_{post} is energy released in a region comprised between δ_{peak} and δ. The related parameters in the Eq. (1) can be obtained from the typical load-deflection curve, as shown in Fig. 12.

Fig. 13 depicts the relative increment of PCS (respect to the PCS of the reference RCP) for vertical displacements of the crown ranging from 20 mm (onset of cracking) to 100 mm. The results evidence that B6P0 and B0P6 pipes presented a decreasing tendency of the relative-to-RCP PCS, this being, however, positive (thus superior to PCS of RCP) through the whole range of displacements analyzed.

The pipe B2P4 presented an increasing tendency of this parameter most probably as a results of the synergetic contribution of the BFs and the PPFs that led to a major number of cracks respect to the other pipes (Table 6) and, consequently, a greater ductility and bending moment redistribution capacity.

3.3. Failure modes

The failure was governed by bending in the 4 tested pipes (Fig. 14), with high ductility and distributed cracking around the main cracks. These main cracks (crown, invert and springline) behaved as plastic hinges that controlled the resistant mechanism through the steel reinforcement. The failure was caused by concrete crushing due to excessive compression at the hinges, this phenomenon being symptom of ductility provided by the steel cage and fiber reinforcement.

It must be remarked that the standard RCP (B0P0) evidenced concrete spalling (Fig. 14(a)) due to the inwards pressure of the steel bars. Contrarily, the tested FRCPs showed a decreasing to tendency to this phenomenon since fibers effectively prevented concrete pieces from spalling and debonding of the pipe. Specifically, for the micro BF reinforced concrete pipe specimen (B6P0), the spalling decreased to some extent and the dropping blocks were less in number and smaller in size than those observed for the pipe B0P0 (Fig. 14(c)). Likewise, for the PPF reinforced concrete specimen (B0P6) and hybrid fiber reinforced concrete specimen (B2P4), no concrete spalling was detected as shown in Figs. 14(b)and 14(d). Hence, the size of the fiber plays a relevant role in the concrete spalling mechanism, macrofibers (polypropylene) being those more effective for controlling this phenomenon.

4. Conclusions

An experimental program consisting in producing a standard steel-cage reinforced concrete pipe (RCP), taken as reference, and fiber reinforced concrete pipes (FRCPs) reinforced with the same steel-cage configuration and basalt microfibers (BFs), polypropylene macrofibers (PPFs) and a hybridization on both fibers. The internal diameter of the pipes was 1000 mm, and these were subjected to the three-edge bearing test load configuration and monitored to measure deflections and crack patterns up failure. The results obtained and the analyses carried out allows drawing the following conclusions:

(1) The pre-cracking response of the pipes were unsensitive to the addition of fibers; however, this contributed in controlling effectively the cracks patterns up to failure loads. In this regard, the $D_{0.3}$ of B6P0 (6 kg/m^3 BFs), B0P6 (6 kg/m^3 PPFs) and B2P4 (2 kg/m^3 and 4 kg/m^3 of BFs and PPFs,

respectively) resulted to be 17.4%, 30.9% and 34.1% superior to the $D_{0.3}$ reached by the pipe B0P0 (RCP). The inclusion of the fibers to the RCP allowed to reach the pipe strength class V.

(2) D_u increased from 12.5% (B6P0) to 31.0% (B2P4) respect to that obtained for the RCP. An structural positive synergetic effect due to hybridization of the fibers was evidences, this being reflected in an increase of D_u for the pipe B2P4 of 16.0% and 4.1% respect to the pipes B6P0 and B0P6, respectively.

(3) The FRCPs presented greater post-cracking energy absorption (PCS) respect to that observed for the reference RCP. PCS tendency was decreasing for the pipes B6P0 and B0P6 whilst the pipe B2P4 presented an increasing tendency due to the synergetic contribution of the BFs and the PPFs.

(4) Fibers effectively prevented concrete pieces from spalling and debonding of the pipe, PPFs being those more effective for controlling this phenomenon.

In this experimental program a limited number of specimens were tested, making the conclusions applicable to pipes with the similar diameter and reinforcement configurations. To generalize the conclusions, an extensive numerical program was carried out to obtain the mechanical response of pipes with other diameters and reinforcement configurations. The experimental results were used to validate the finite element model developed. The results and conclusions derived from this numerical research are presented in another paper.

Acknowledgments

This work is supported by the National Key Research and Development Program of China (2018YFC1504802), Natural Science Foundation Project of Chongqing (cstc2018jscx-mszdX0071), Postgraduate Research Innovation Project of Chongqing (CYS19005, CYS18026). In addition, Prof. Albert de la Fuente also wants to express his gratitude to the Spanish Ministry of Science and Innovation for the financial support received under the scope of the project CREEF (PID2019-108978RB-C32).

References

1. Rikabi F T, Sargand S M, Kurdziel J, Hussein H H. Experimental investigation of thin-wall synthetic fiber-reinforced concrete pipes. ACI Structural Journal, 2018, 115(6): 1671-1681.

2. Abolmaali A, Mikhaylova A, Wilson A, Lundy J. Performance of steel fiber-reinforced concrete pipes. Transportation Research Record, 2012, 2313(1): 168-177.

3. ASTM C76-19a, Standard Specification for Reinforced Concrete Culvert, Storm Drain, and Sewer Pipe. ASTM International, West Conshohocken, PA, 2019.
4. AS 4139:2003, Fiber-reinforced concrete pipes and fittings. 2003.
5. EN 1916:2002, Concrete pipes and fittings, unreinforced, steel fiber and reinforced. 2002.
6. UNE-EN 127916:2008, Concrete pipes and fittings, unreinforced, steel fiber and reinforced. National complement to the standard UNE-EN 1916:2002, 2008.
7. De la Fuente A, Escariz R C, de Figueiredo A D, Molins C, Aguado A. A new design method for steel fibre reinforced concrete pipes. Construction and Building Materials, 2012, 30: 547-555.
8. De la Fuente A, de Figueiredo A D, Aguado A, Molins C, Neto P J C. Experimentation and numerical simulation of steel fibre reinforced concrete pipes. Materiales De Construccion, 2011, 61(302): 275-288.
9. Abolmaali A, Mikhaylova A, Wilson A, Lundy J. Performance of Steel Fiber–Reinforced Concrete Pipes. Transportation Research Record, 2012, 2313(1): 168-177.
10. Haktanir T, Ari K, Altun F, Karahan O. A comparative experimental investigation of concrete, reinforced-concrete and steel-fibre concrete pipes under three-edge-bearing test. Construction and Building Materials, 2007, 21(8): 1702-1708.
11. Mohamed N, Soliman A M, Nehdi M L. Full-scale pipes using dry-cast steel fibre-reinforced concrete. Construction and Building Materials, 2014, 72: 411-422.
12. Mohamed N, Soliman A M, Nehdi M L. Mechanical performance of full-scale precast steel fibre-reinforced concrete pipes. Engineering Structures, 2015, 84: 287-299.
13. Mu R, Xue Y, Qing L, Li H, Zhao Y, Zhou J, Su J. Preparation and mechanical performance of annularly aligned steel fiber reinforced cement-based composite pipes. Construction and Building Materials, 2019, 211: 167-173.
14. Song P S, Hwang S. Mechanical properties of high-strength steel fiber-reinforced concrete. Construction and Building Materials, 2004, 18(9): 669-673.
15. Hannant D J. Durability of polypropylene fibers in portland cement-based composites: eighteen years of data. Cement and Concrete Research, 1998, 28(12): 1809-1817.
16. Mu B, Meyer C, Shimanovich S. Improving the interface bond between fiber mesh and cementitious matrix. Cement and Concrete Research, 2002, 32(5): 783-787.
17. Richardson A E. Electrical properties of Portland cement, with the addition of polypropylene fibres

– regarding durability. Structural Survey, 2004, 22(3): 156-163.

18. Buratti N, Mazzotti C, Savoia M. Post-cracking behaviour of steel and macro-synthetic fibre-reinforced concretes. Construction and Building Materials, 2011, 25(5): 2713-2722.

19. Buratti N, Mazzotti C. Experimental tests on the effect of temperature on the long-term behaviour of macrosynthetic Fibre Reinforced Concretes. Construction and Building Materials, 2015, 95: 133-142.

20. Rostami R, Zarrebini M, Abdellahi S B, Mostofinejad D, Abtahi S M. Investigation of flexural performance of concrete reinforced with indented and fibrillated macro polypropylene fibers based on numerical and experimental comparison. Structural Concrete, n/a(n/a). https://doi.org/10.1002/suco.201900374.

21. Mudadu A, Tiberti G, Plizzari G A, Morbi A. Post-cracking behavior of polypropylene fiber reinforced concrete under bending and uniaxial tensile tests. Structural Concrete, 2019, 20(4): 1411-1424.

22. Wang Q, Ding Y, Zhang Y, Castro C. Effect of macro polypropylene fiber and basalt fiber on impact resistance of basalt fiber-reinforced polymer-reinforced concrete. Structural Concrete, 2020, n/a(n/a). https://doi.org/10.1002/suco.201900482.

23. Figueiredo A. Evaluation of the test method for crushing strength of steel fiber reinforced concrete pipes. 2008.

24. Figueiredo A, De la Fuente A, Aguado A, Molins C, Neto P. Steel fiber reinforced concrete pipes. Part 1: technological analysis of the mechanical behavior. Revista IBRACON de Estruturas e Materiais, 2012, 5: 1-11.

25. De la Fuente A, Figueiredo A, Aguado A, Molins C, Neto P. Steel fiber reinforced concrete pipes. Part 2: Numerical model to simulate the crushing test. Revista IBRACON de Estruturas e Materiais, 2012, 5: 12-25.

26. De la Fuente A, Escariz R C, de Figueiredo A D, Aguado A. Design of macro-synthetic fibre reinforced concrete pipes. Construction and Building Materials, 2013, 43: 523-532.

27. Wilson A, Abolmaali A. Performance of Synthetic Fiber-Reinforced Concrete Pipes. Journal of Pipeline Systems Engineering and Practice, 2014, 5(3): 7.

28. Mohamed N, Nehdi M L. Rational finite element assisted design of precast steel fibre reinforced concrete pipes. Engineering Structures, 2016, 124: 196-206.

29. Monte R, De la Fuente A, Figueiredo A, Aguado A. Barcelona Test as an Alternative Method to Control and Design Fiber-Reinforced Concrete Pipes. ACI Structural Journal, 2016, 113: 1175-1184.
30. Zdrenghea D. Steel Fibers Reinforced Concrete Pipes - Experimental Tests and Numerical Simulation. IOP Conference Series: Materials Science and Engineering, 2017, 245: 022032.
31. Al Rikabi FT, Sargand SM, Khoury I, Kurdziel J, Hussein HH, Ahmed S. Thin-Wall Synthetic Fiber Reinforced Concrete Pipe Performance under Cyclic Loading. Pipelines 2019: Multidisciplinary Topics, Utility Engineering, and Surveying - Proceedings of Sessions of the Pipelines 2019 Conference. 2019:547-554.
32. Al Rikabi F T, Sargand S M, Kurdziel J. Evaluation of synthetic fiber reinforced concrete pipe performance using three-edge bearing test. Journal of Testing and Evaluation, 2019, 47(2) :942-958.
33. Lee S, Park Y, Abolmaali A. Investigation of Flexural Toughness for Steel-and-Synthetic-Fiber-Reinforced Concrete Pipes. Structures, 2019, 19: 203-211.
34. Peyvandi A, Soroushian P, Jahangirnejad S. Enhancement of the structural efficiency and performance of concrete pipes through fiber reinforcement. Construction and Building Materials, 2013, 45: 36-44.
35. Peyvandi A, Soroushian P, Jahangirnejad S. Structural Design Methodologies for Concrete Pipes with Steel and Synthetic Fiber Reinforcement. Aci Structural Journal, 2014, 111: 83-92.
36. Park Y, Abolmaali A, Attiogbe E, Lee S-H. Time-Dependent Behavior of Synthetic Fiber–Reinforced Concrete Pipes under Long-Term Sustained Loading. Transportation Research Record: Journal of the Transportation Research Board, 2014, 2407(1): 71-79.
37. Park Y, Abolmaali A, Beakley J, Attiogbe E. Thin-walled flexible concrete pipes with synthetic fibers and reduced traditional steel cage. Engineering Structures, 2015, 100: 731-741.
38. Park Y, Abolmaali A, Mohammadagha M, Lee S. Structural performance of dry-cast rubberized concrete pipes with steel and synthetic fibers. Construction and Building Materials, 2015, 77: 218-226.
39. Li B, Chi Y, Xu L, Shi Y, Li C. Experimental investigation on the flexural behavior of steel-polypropylene hybrid fiber reinforced concrete. Construction and Building Materials, 2018, 191: 80-94.
40. Yoo D-Y, Kim M-J. High energy absorbent ultra-high-performance concrete with hybrid steel and polyethylene fibers. Construction and Building Materials, 2019, 209: 354-363.

41. Lee S, Park Y, Abolmaali A. Investigation of Flexural Toughness for Steel-and-Synthetic-Fiber-Reinforced Concrete Pipes. Structures, 2019, 19: 203-211.

42. Sim J, Park C, Moon D Y. Characteristics of basalt fiber as a strengthening material for concrete structures. Composites Part B: Engineering, 2005, 36(6): 504-512.

43. Kizilkanat A B, Kabay N, Akyüncü V, Chowdhury S, Akça A H. Mechanical properties and fracture behavior of basalt and glass fiber reinforced concrete: An experimental study. Construction and Building Materials, 2015, 100: 218-224.

44. Jiang C, Fan K, Wu F, Chen D. Experimental study on the mechanical properties and microstructure of chopped basalt fibre reinforced concrete. Materials & Design, 2014, 58: 187-193.

45. Branston J, Das S, Kenno S Y, Taylor C. Mechanical behaviour of basalt fibre reinforced concrete. Construction and Building Materials, 2016, 124: 878-886.

46. Borhan T M. Properties of glass concrete reinforced with short basalt fibre. Materials & Design, 2012, 42: 265-271.

47. Fu Q, Niu D T, Zhang J, Huang D G, Hong M S. Impact response of concrete reinforced with hybrid basalt-polypropylene fibers. Powder Technology, 2018, 326: 411-424.

48. Fu Q, Niu D, Li D, Wang Y, Zhang J, Huang D. Impact characterization and modelling of basalt–polypropylene fibre-reinforced concrete containing mineral admixtures. Cement and Concrete Composites, 2018, 93: 246-259.

49. Zhang H, Wang L, Bai L, Addae M, Neupane A. Research on the impact response and model of hybrid basalt-macro synthetic polypropylene fiber reinforced concrete. Construction and Building Materials, 2019, 204: 303-316.

50. Smarzewski P. Flexural Toughness of High-Performance Concrete with Basalt and Polypropylene Short Fibres. Advances in Civil Engineering, 2018, 8: 5024353.

51. Smarzewski P. Influence of basalt-polypropylene fibres on fracture properties of high performance concrete. Composite Structures, 2019, 209: 23-33.

52. Lopresto V, Leone C, De Iorio I. Mechanical characterisation of basalt fibre reinforced plastic. Composites Part B: Engineering, 2011, 42(4): 717-723.

53. Deng Z, Liu X, Yang X, Liang N, Yan R, Chen P, Miao Q, Xu Y. A study of tensile and compressive properties of hybrid basalt-polypropylene fiber-reinforced concrete under uniaxial loads. Structural Concrete, n/a(n/a). https://doi.org/10.1002/suco.202000006.

54. Pujadas P, Blanco A, Cavalaro S, Aguado A. Plastic fibres as the only reinforcement for flat suspended slabs: Experimental investigation and numerical simulation. Construction and Building Materials, 2014, 57: 92-104.

55. Pujadas P, Blanco A, Cavalaro S, de la Fuente A, Aguado A. The need to consider flexural post-cracking creep behavior of macro-synthetic fiber reinforced concrete. Construction and Building Materials, 2017, 149: 790-800.

56. Banthia N, Trottier J F. Test methods for flexural toughness characterization of fiber-reinforced concrete - some concerns and a proposition. Aci Materials Journal, 1995, 92(1): 48-57.

List of figure captions

Figure 1 Typical thrust phase of a pipe jacketing system

Figure 2 Types of cracks: (a) flexural crack with carbonate crystal precipitate; (b) water seepage across a crack caused by the jack thrust

Figure 3 External shapes of fibers: (a) PPFs; (b) BFs

Figure 4 Layout of reinforcement skeleton

Figure 5 Self-designed mold for producing pipe: (a) external connection; (b) internal connection. (1 horizontal base; 2-external positioning device; 3-fastening bolt; 4-wooden blocks; 5-iron hoop; 6-external reinforcing formwork; 7-external annular iron strap; 8-external vertical wood; 9-annular gap; 10-internal vertical wood; 11-rubber strip; 12-nail; 13-internal annular iron strap; 14-internal reinforcing formwork; 15-internal positioning device.)

Figure 6 Pipe production processes: (a) mold making; (b) reinforcement cage installation and positioning; (c) installation and positioning of the outer mold; (b) completion and maintenance of pipe

Figure 7 Diagram of three-edge bearing test: (a) lateral view; (b) front view

Figure 8 Part of the test processes: (a) installation and preparation of specimen; (b) application of load; (c) observation and mark of cracks; (d) data collection and recording

Figure 9 DL vs vertical deflection of pipes

Figure 10 Crack patterns after unloading (post-failure): (a) B0P0; (b) B0P6; (c) B6P0 and (d) B2P4

Figure 11 DL vs maximum crack width (crown, in all cases)

Figure 12 Typical load-deflection curve

Figure 13 PCS increment ratio of the FRCPs respect to the RCP

Figure 14 Failure modes of pipes: (a) B0P0: pipe without fiber; (b) B0P6: pipe with PPF; (c) B6P0: pipe with BF; (b) B2P4: pipe with B-PP hybrid fiber

Figure 1 Typical thrust phase of a pipe jacketing system

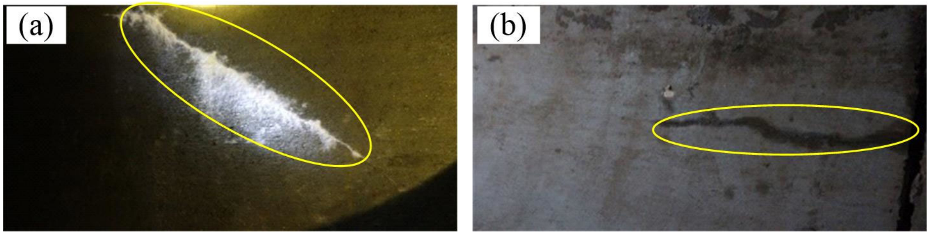

Figure 2 Types of cracks: (a) flexural crack with carbonate crystal precipitate; (b) water seepage across a crack caused by the jack thrust

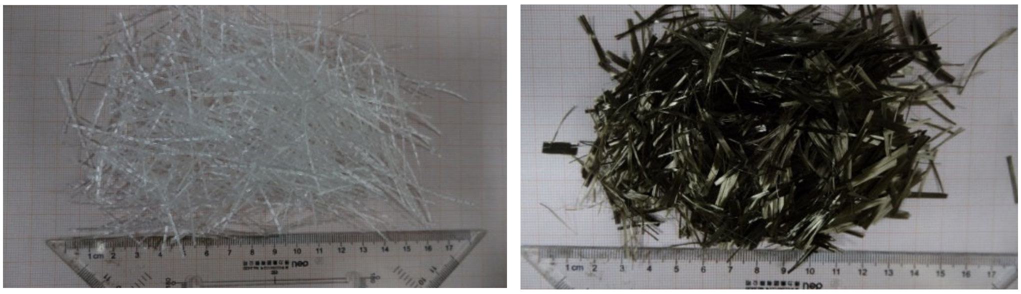

(a) (b)

Figure 3 External shapes of fibers: (a) PPFs; (b) BFs

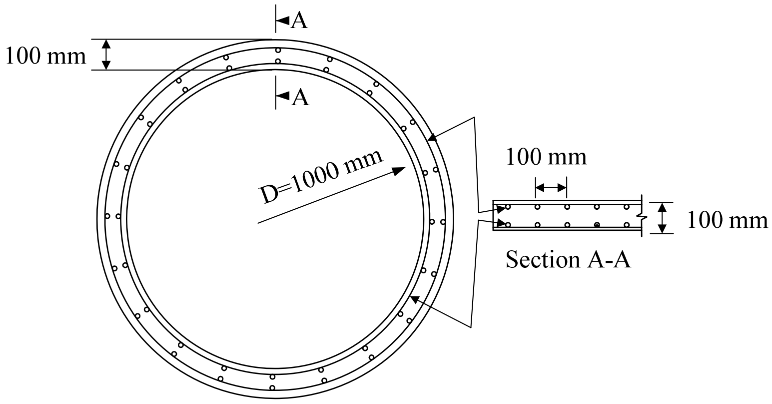

Figure 4 Layout of reinforcement skeleton

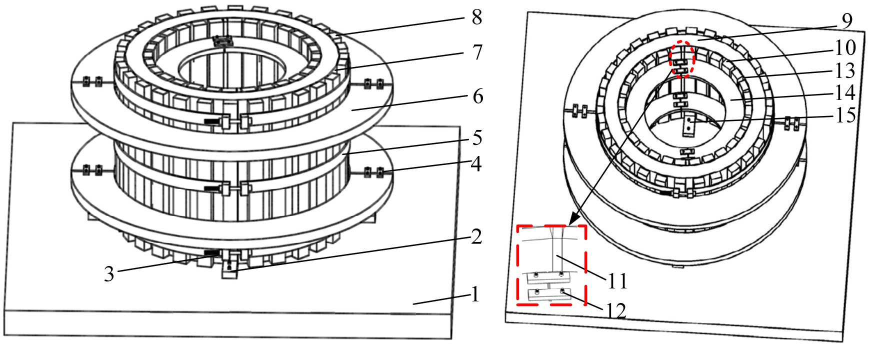

(a) (b)

Figure 5 Self-designed mold for producing pipe: (a) external connection; (b) internal connection. (1 horizontal base; 2-external positioning device; 3-fastening bolt; 4-wooden blocks; 5-iron hoop; 6-external reinforcing formwork; 7-external annular iron strap; 8-external vertical wood; 9-annular gap; 10-internal vertical wood; 11-rubber strip; 12-nail; 13-internal annular iron strap; 14-internal reinforcing formwork; 15-internal positioning device.)

Figure 6 Pipe production processes: (a) mold making; (b) reinforcement cage installation and positioning; (c) installation and positioning of the outer mold; (b) completion and maintenance of pipe

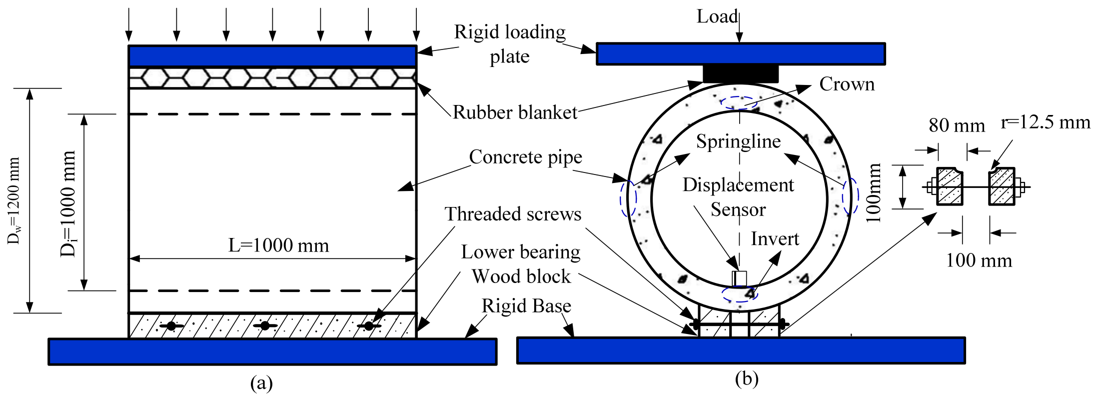

Figure 7 Diagram of three-edge bearing test: (a) lateral view; (b) front view

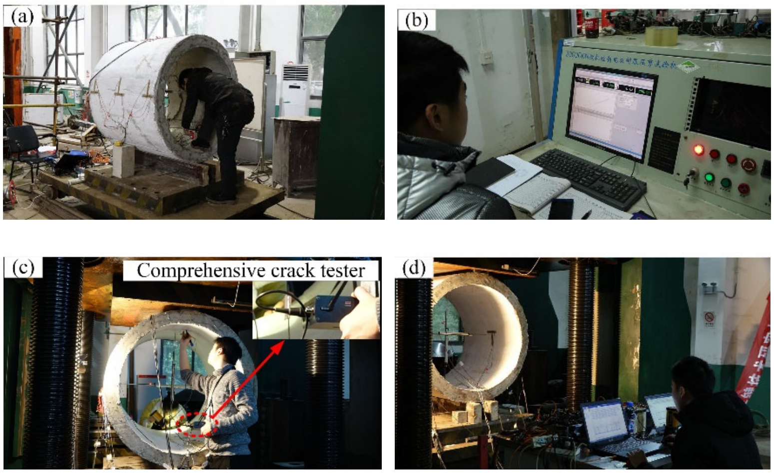

Figure 8 Part of the test processes: (a) installation and preparation of specimen; (b) application of load; (c) observation and mark of cracks; (d) data collection and recording

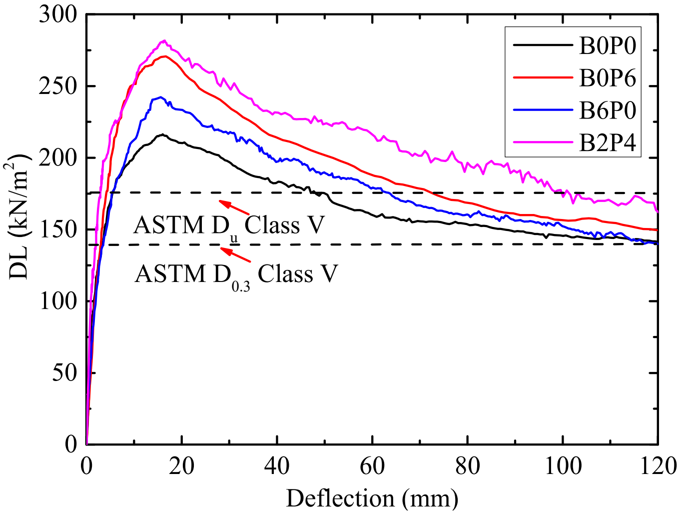

Figure 9 DL vs vertical deflection of pipes

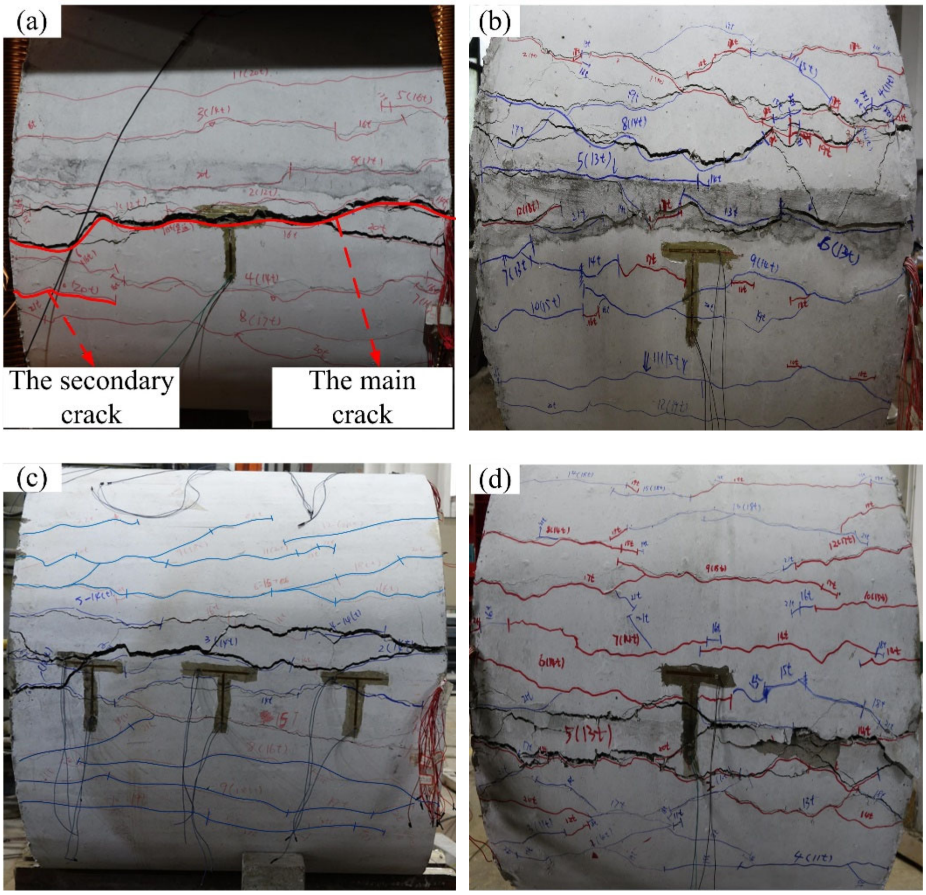

Figure 10 Crack patterns after unloading (post-failure): (a) B0P0; (b) B0P6; (c) B6P0 and (d) B2P4

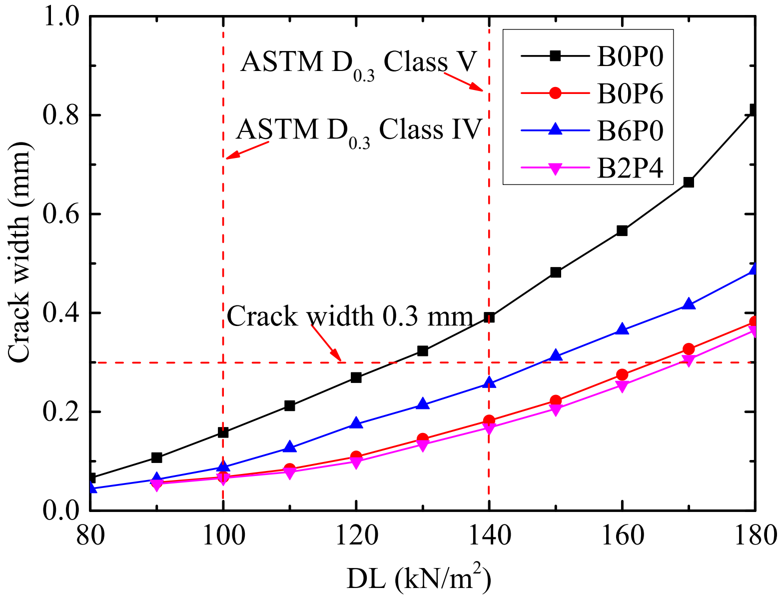

Figure 11 DL vs maximum crack width (crown, in all cases)

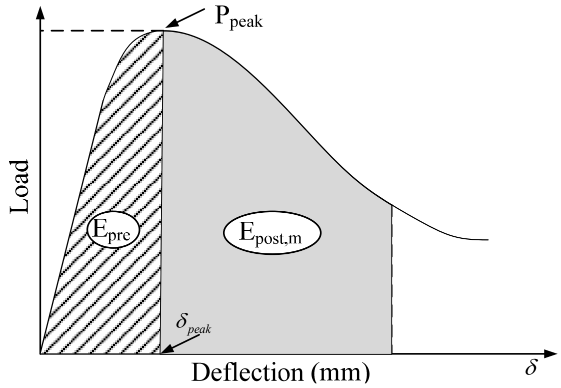

Figure 12 Typical load-deflection curve

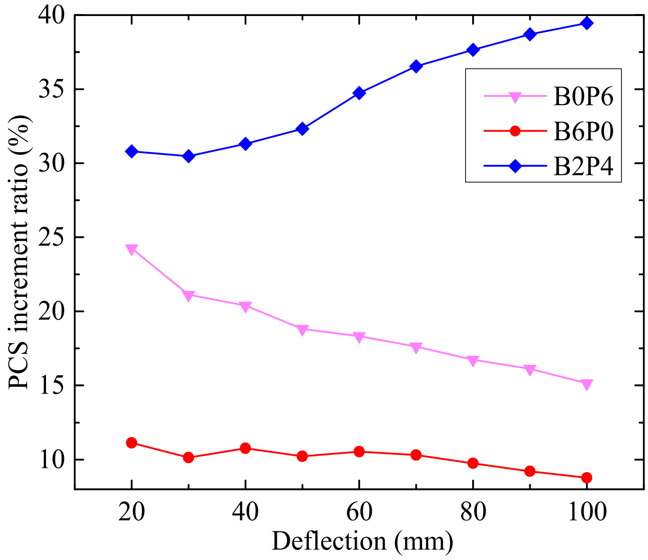

Figure 13 PCS increment ratio of the FRCPs respect to the RCP

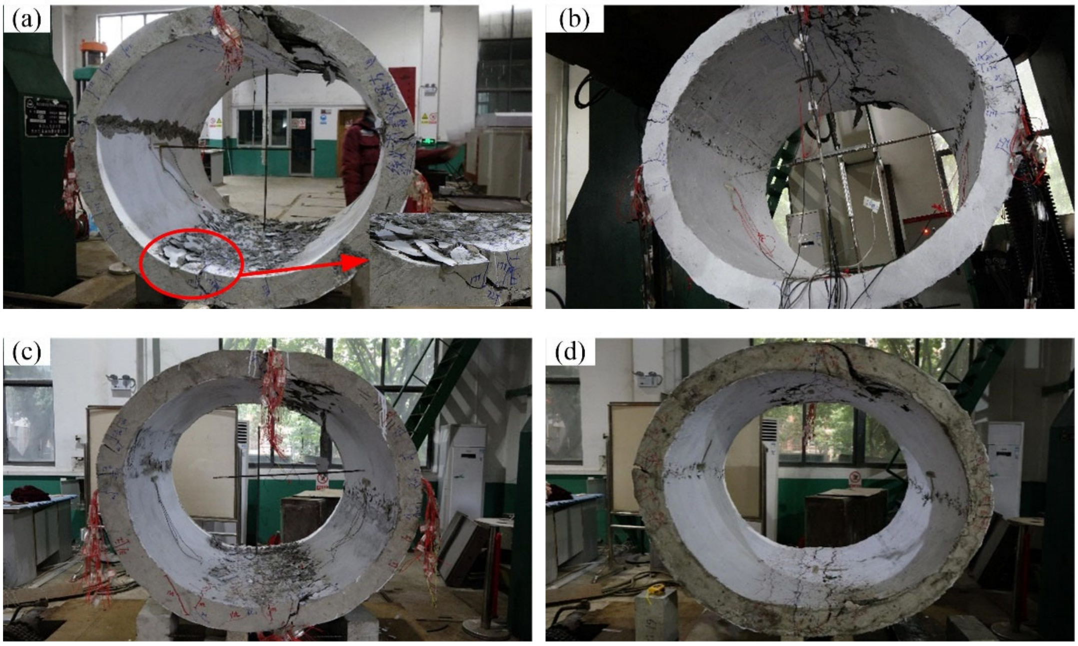

Figure 14 Failure modes of pipes: (a) B0P0: pipe without fiber; (b) B0P6: pipe with PPF; (c) B6P0: pipe with BF; (b) B2P4: pipe with B-PP hybrid fiber

List of table captions

Table 1 Numerical and experimental programs related to FRCPs

Elements	f_c (MPa)	Dimensions (mm) Di-h/b	Reinforcement: Steel cage (cm^2 /m)	Reinforcement: Fiber (% in volume)	Φ_f/λ_f	Type of fibers	Tests: Type	Tests: No.	Numerical Simulation	Ref.
PCP	38	500-60/1500	-	-	-	-	IT	3	None	10
RCP			Si: 5.1					3		
SFRCP			-	0.25 & 0.51	0.75/80	SF: hooked-end		6		
					0.75/40			6		
SFRCP	*	800-*/2000	-	0.13 & 0.25 & 0.51	0.75/80	SF: hooked-end	TEBT	20	None	23
SFRCP	*	600-72/2500	-	0.13 & 0.25 & 0.51	0.75/80	SF: hooked-end	TEBT	18	MAP	8
PCP	35~45	1000-90/1500	-	-	-	-	TEBT	3	MAP	7
SFRCP				0.25 & 0.31 & 0.44	0.75/80	SF: hooked-end		9		
SFRCP	50	600-72/2500	-	0.13 & 0.25 & 0.51	0.75/60	SF: hooked-end	TEBT	24	MAP	24, 25
SFRCP	*	400~1200-58~131/*	-	0.17 & 0.33 & 0.50 & 0.66 & 0.83	0.54/65	SF: hooked-end	TEBT	66	None	2
PCP	*	1000-80/1500	-	-	-	-	TEBT	3	MAP	26
PFRCP				0.33 & 0.49 & 0.66	0.9/60	PPF: embossed surface		12		
RCP	＞27	375~600-56~100/*	Regular	-	-	-	TEBT	*	None	27
PFRCP			-	0.26&0.39&0.52&0.65&0.78&1.04&1.17	0.82/66	PPF: embossed surface		93		
PCP	66	450-82/2450	-	-	-	-	TEBT	3	3D-FE elastoplastic	12, 28
	64.8	600-94/2450						3		
RCP	47	450-82/2450	Regular					3		
	43.8	600-94/2450						3		
SFRCP	25~30.3	600-62/1500	-	0.13 & 0.26	0.62/48	SF: hooked end	TEBT	8	MAP	29

PFRCP				0.26 & 0.52	0.32/169	PPF: monofilament		5		
SFFRCP	*	1410-140/1500 2200-160/2000	-	0.45	/	/	TEBT TEBT	1 1		30
PFRCP	*	1200-50/* 1500-63/*	Si:5.7 □ Si:10.2 □ Si:5.7 □ Si:8.9 □	1.0	0.82/66	/	TEBT	1 1 1 1	None	1
PFRCP	47.35	1200-50/*	Si:10.2 □	1.0	0.91/60	/	TEBT	1	None	31
PCP		-	-	-	-	-		3		
PFRCP	*	600-75/2400 1200-125/1200 1200-125/1200	- Si:1.5□ - Si:5.1 □ Si:5.1	1.0 & 2.0 1.0 & 2.0 0.5 & 1.0 0.5 & 1.0 & 1.5 1.0 & 1.5 & 2.0	0.91/60	*	TEBT	4 3 6 11 9	None	32
SFRCP	33	450~900-63~100/*	-	0.15 & 0.2 & 0.3 & 0.4	0.538/65	SF: hooked at the ends	TEBT	22	None	33
PFRCP		375~900-56~100/*		0.15 & 0.23 & 0.31 & 0.4 & 0.46	0.82/66	PPF: hooked-shaped ends		40		

Note：* means lack of information; Di is internal pipe diameter; h is the pipe wall thickness; b is the pipe length; Φ_f is the diameter of the fiber; λ_f is the fiber aspect ratio; Ref. is reference; PCP is plain concrete pipe; Si is single reinforcement cage; IT is impact test; TEBT is three edge bearing tests; PPF is polypropylene fiber; MAP is the numerical model for the analysis of pipes.

Table 2 Geometrical and mechanical properties of the selected fibers

	BF	PPF
Diameter (mm)	0.013	0.8
Length (mm)	19	50
Shape	straight	embossed
Tensile strength (MPa)	3300-4500	706
Elastic modulus (GPa)	95-115	7.4
Density (g/cm^3)	2.75	0.95
Elongation (%)	2.4-3.0	10

Table 3 Concrete mixture properties

Material	Mass(kg/m^3)
Cement	375
Coarse aggregate 10~20mm	545
Coarse aggregate 5~10mm	545
Sand	850
Water	135
Water reducer	3.75

Table 4 Details of produced pipes

Pipe number	Code	Fiber content in kg/m³ (% in volume)		f_{cc} (MPa)	f_{ct} (MPa)
		BF	PPF		
1(control)	B0P0	0 (0%)	0 (0%)	47.1	2.65
2	B6P0	6 (0.22%)	0 (0%)	50.4	2.76
3	B0P6	0 (0%)	6 (0.63%)	49.0	3.15
4	B2P4	2 (0.07%)	4 (0.42%)	53.7	3.29

BXPY; B: BF; X: BF content (kg/m^3); P: PPF; Y: PPF content (kg/m^3)

Table 5 Strength requirement by pipe class based on ASTM C76 [3]

Pipe class	DL (kN/m^2)	
	$D_{0.3}$ (service)	D_u (ultimate)
I	40	60
II	50	75
III	65	100
IV	100	150
V	140	175

Table 6 Information of cracks for each key section of the four pipes when subjected to the service load ($D_{0.3}$ = 140 kN/m^2)

Information of cracks		Pipe Code			
		B0P0	B0P6	B6P0	B2P4
Crown	Number (No.)	2	4	3	5
	Se. (No./av.)	1/0.11	3/0.05	2/0.07	4/0.04
	Ma. (No./max.)	1/0.39	1/0.18	1/0.26	1/0.17
Invert	Number	2	4	3	4
	Se. (No./av.)	1/0.10	2/0.05	3/0.06	3/0.04
	Ma. (No./max.)	1/0.36	1/0.17	1/0.23	1/0.15
Left	Number	5	8	5	11
springline	Se. (No./av.)	4/0.07	7/0.04	4/0.05	10/0.03
	Ma. (No./max.)	1/0.25	1/0.12	1/0.17	1/0.10
Right	To.	4	9	5	12
springline	Se. (No./av.)	3/0.07	8/0.04	4/0.05	11/0.03
	Ma. (No./maxi.)	1/0.23	1/0.12	1/0.17	1/0.10

Note: "Se. (No./av.)"secondary cracks (number/average crack with (mm)); "Ma. (No./maxi.)" means main crack (number/maximum crack with (mm))